Bioelectrochemistry 99 (2014) 8–16

Contents lists available at ScienceDirect

Bioelectrochemistry

journal homepage: www.elsevier.com/locate/bioelechem

Bioelectrochemical sensing of promethazine with bamboo-type multiwalled carbon nanotubes dispersed in calf-thymus double stranded DNA

Emiliano N. Primo [a], M. Belén Oviedo [b], Cristián G. Sánchez [b], María D. Rubianes [a,*], Gustavo A. Rivas [a,*]

[a] INFIQC (CONICET – Universidad Nacional de Córdoba), Departamento de Fisicoquímica, Facultad de Ciencias Químicas, Universidad Nacional de Córdoba, Ciudad Universitaria, 5000 Córdoba, Argentina

[b] INFIQC (CONICET – Universidad Nacional de Córdoba), Departamento de Matemática y Física, Facultad de Ciencias Químicas, Universidad Nacional de Córdoba, Ciudad Universitaria, 5000 Córdoba, Argentina

ARTICLE INFO

Article history:
Received 6 January 2014
Received in revised form 3 May 2014
Accepted 20 May 2014
Available online 2 June 2014

Keywords:
Bamboo carbon nanotube
Dispersion
Double stranded DNA
Intercalation
Promethazine
Electrochemical (bio)sensor

ABSTRACT

We report the quantification of promethazine (PMZ) using glassy carbon electrodes (GCE) modified with bamboo-like multi-walled carbon nanotubes (bCNT) dispersed in double stranded calf-thymus DNA (dsDNA) (GCE/bCNT-dsDNA). Cyclic voltammetry measurements demonstrated that PMZ presents a thin film-confined redox behavior at GCE/bCNT-dsDNA, opposite to the irreversibly-adsorbed behavior obtained at GCE modified with bCNT dispersed in ethanol (GCE/bCNT). Differential pulse voltammetry-adsorptive stripping with medium exchange experiments performed with GCE/bCNT-dsDNA and GCE modified with bCNTs dispersed in single-stranded calf-thymus DNA (ssDNA) confirmed that the interaction between PMZ and bCNT-dsDNA is mainly hydrophobic. These differences are due to the intercalation of PMZ within the dsDNA that supports the bCNTs, as evidenced from the bathochromic displacement of UV–Vis absorption spectra of PMZ and quantum dynamics calculations at DFTB level. The efficient accumulation of PMZ at GCE/bCNT-dsDNA made possible its sensitive quantification at nanomolar levels (sensitivity: $(3.50 \pm 0.05) \times 10^8$ μA·cm $^{-2}$·M $^{-1}$ and detection limit: 23 nM). The biosensor was successfully used for the determination of PMZ in a pharmaceutical product with excellent correlation.

1. Introduction

The knowledge generated in the last years, regarding the synthesis and manipulation of materials at the nanometer scale and the discovering of their exciting properties, has made possible the spectacular growth of the Nanosciences [1–3]. Since 1991, carbon nanotubes (CNT) have received great attention due to their outstanding properties; however, they still surprise us with their unlimited applications in different disciplines [4–6].

Among CNTs, the bamboo-like multi-walled carbon nanotubes (bCNT), a poorly studied allotrope, consist of concentric rolled-up graphene sheets with transverse walls located along the tubes [7,8]. This increased density of edge-plane defects provides bCNTs of excellent electrocatalytic properties. The association of these properties with the high adsorption capacity and conductivity inherent to CNTs makes them a very important material for the development of electrochemical sensors [9–11].

Since CNTs are insoluble in all the solvents, their functionalization is highly required to rationally design supramolecular architectures that allow the development of electrochemical (bio)sensors [12,13]. The non-covalent functionalization of CNTs with biological molecules improves its biocompatibility, solubility and selectivity. Nevertheless, the immobilization of biomolecules at CNTs is a critical step. In this sense, a compromise between the efficient bio-modification of the nanomaterial and the preservation of the structure and properties of the biomolecule is highly required. We recently proposed the use of double stranded calf-thymus DNA (dsDNA) to efficiently disperse bCNT and we demonstrated that the drastic treatment for dispersing them (45 min sonication in a 50% v/v ethanol:water solution) produces a partial denaturation and a decrease in the length of the dsDNA that facilitates the dispersion of CNTs and makes possible an efficient electrooxidation of guanine residues at glassy carbon electrode (GCE) modified with the dispersions [14]. The crucial question is whether the dsDNA that supports the bCNTs keeps the bio-affinity properties for further development of affinity biosensors.

In the last two decades there has been increasing interest in the use of DNA for the development of affinity biosensors [15–25]. The detection of small compounds (pollutants, drugs) using electrochemical DNA-biosensors based on the redox signal of the compound or the

* Corresponding authors. Tel.: +54 351 5353866; fax: +54 351 4334188.
E-mail addresses: rubianes@fcq.unc.edu.ar (M.D. Rubianes), grivas@fcq.unc.edu.ar (G.A. Rivas).

http://dx.doi.org/10.1016/j.bioelechem.2014.05.002
1567-5394/

intrinsic changes in the DNA signal has been extensively explored [21–25].

Promethazine (PMZ) (Scheme 1) is an antihistaminic and neuroleptic drug. Early studies suggested that the phenothiazinium radical cation, obtained by enzymatic oxidation of PMZ, can irreversibly interact with dsDNA mainly by intercalation [26,27]. There are several works based on the interaction of PMZ with dsDNA immobilized at different electrodes for the electrochemical quantification of PMZ in pharmaceutical formulations [28–31]. However, even when the properties of PMZ as intercalator are known, no critical studies have been performed about this interaction with dsDNA [32]. To the best of our knowledge, almost no systematic studies have been performed about the change in dsDNA intercalation capability when immobilizing dsDNA at electrode surfaces.

The main motivation of this work was to answer a key question regarding the bioaffinity properties of the dsDNA that supports the bCNT at GCE/bCNT-dsDNA and the analytical usefulness of this electrode. It is focused on the study of the interaction of PMZ with GCE/bCNT-dsDNA and the development of a new bioaffinity platform for the sensitive electrochemical quantification of PMZ.

In the following sections we evaluate the interaction between PMZ and the dsDNA that supports the bCNTs from the electrochemical activity of PMZ at GCE/bCNT-dsDNA using differential pulse voltammetry (DPV) adsorptive stripping with medium exchange. A comparison is also performed using GCE modified with bCNT dispersed in ethanol:water (GCE/bCNT) or in ssDNA (GCE/bCNT-ssDNA).

The intercalation of PMZ within dsDNA and bCNT-dsDNA was critically evaluated by using UV–Vis spectroscopy and quantum dynamics calculations at DFTB level. The analytical usefulness of GCE/bCNT-dsDNA for the sensitive quantification of PMZ in a pharmaceutical formulation is also discussed.

2. Experimental

2.1. Apparatus

The electrochemical measurements were performed with an Autolab (PGSTAT 128N EcoChemie) potentiostat. The electrodes were inserted into the cell through holes in its Teflon cover. A platinum wire and Ag/AgCl, 3 M NaCl (BAS) were used as counter and reference electrodes, respectively. All potentials are referred to the latter.

UV–Vis experiments were carried out with a Shimadzu UV1700 Pharma spectrometer.

2.2. Reagents

Calf-thymus double stranded DNA (dsDNA, Catalog number D 4522), calf-thymus single stranded DNA (ssDNA, Catalog number D 8899) and promethazine hydrochloride (PMZ, Catalog number P 4651) were purchased from Sigma. Bamboo-like multi-walled carbon nanotubes (bCNT, diameter (30 ± 10) nm, length 1–5 μm, 98.92% purity) were obtained from NanoLab (U.S.A.) and used as received. Other chemicals were reagent grade and were used without further purification. Ultrapure water (ρ = 18.2 MΩ·cm) from a Millipore Milli-Q system was used for preparing all the solutions. A 0.200 M acetate buffer solution pH 5.00 was used as supporting electrolyte.

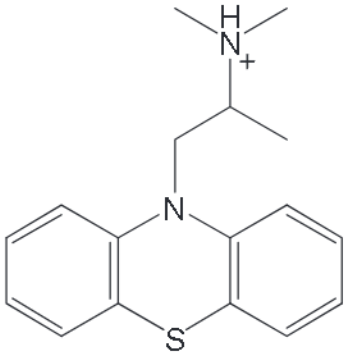

Scheme 1. Promethazine structural formula.

2.3. Preparation of bCNT-modified GCE

2.3.1. Preparation of the dispersions

a) *bCNTs in ethanol:water (bCNT):* the dispersion was obtained by mixing 1.00 mg of bCNT with 1.00 mL of a 50% v/v ethanol:water solution followed by sonication for 45 min.

b) *bCNTs in dsDNA (bCNT-dsDNA):* the dispersion was obtained by mixing 1.00 mg of bCNT with 1.00 mL of a 100 ppm dsDNA solution (prepared in a 50% v/v ethanol:water solution) followed by sonication for 45 min. A similar dispersion was prepared using ssDNA instead of dsDNA. In order to retain only the bCNT dispersed and functionalized with the DNA the dispersions were centrifuged for 15 min at 9000 rpm, and the electrodes were further modified with the supernatant.

2.3.2. Preparation of GCE/bCNT-dsDNA

The GCEs were first polished with alumina slurries of 1.0, 0.3 and 0.05 μm for 1.5 min each and then electrochemically pretreated by performing 10 voltammetric cycles between −0.300 and 0.700 V (vs. Ag/AgCl) in a 0.050 M phosphate buffer solution pH 7.40 at a scan rate of 0.100 $V \cdot s^{-1}$. After that, the electrodes were carefully dried under a N_2 stream.

Once polished and clean, the GCEs were modified by dropping 20 μL of the bCNT-dsDNA dispersion on the top of the surfaces followed by the evaporation of the solvent by exposure to air for 90 min. A similar protocol was employed to prepare GCE/bCNT and GCE/bCNT-ssDNA.

2.4. Procedure

2.4.1. Electrochemical experiments

2.4.1.1. Determination of the electroactive areas. Since the dispersions possess different contents of bCNTs (due to the centrifugation process), the currents were normalized with the electroactive area (A) obtained by chronocoulometry experiments according to Eq. (1):

$$Q_r(t) - \frac{2nFAD_0^{1/2}C_0^*}{\pi^{1/2}}t^{1/2} + Q_{dl} + Q_{ads} \quad (1)$$

where n is the number of exchanged electrons; F is the Faraday constant; A is the electroactive area; D_0 is the diffusion coefficient of the probe; C_0^* is the bulk concentration of the probe and Q_r, Q_{dl} and Q_{ads} are the total charge, the charge due to double layer capacitance and the charge due to adsorption, respectively [33]. The experiments were carried out by applying a potential step of 0.400 V for 4 s in a 5.0×10^{-4} M hydroquinone solution, which was used as the carbonaceous area-sensitive probe [34].

2.4.1.2. Determination of the capacitances. The double layer specific capacitances (C) were obtained from cyclic voltammetry (CV) at different scan rates (v) in the presence of 1.0×10^{-4} M PMZ at 0.360 V, potential at which no faradaic processes occur, according to Eq. (2):

$$j_{dl} - Cv \quad (2)$$

where j_{dl} is the current density due to the charging of the double layer [33].

2.4.1.3. PMZ "stripping" at GCE/CNT-dsDNA. PMZ interaction: performed by immersion of GCE/bCNT-dsDNA (or the particular electrode) in a

0.200 M acetate buffer solution pH 5.00 containing PMZ for 5.0 min at open circuit potential under stirring conditions.

DPV stripping: performed in a 0.200 M acetate buffer solution pH 5.00 by DPV between 0.400 and 1.400 V (vs. Ag/AgCl). DPV parameters: pulse height: 10 mV, amplitude: 50 ms, scan rate: 20 mV · s^{-1}, width: 70 ms and period: 200 ms.

Similar experiments were performed by using GCE, GCE/bCNT and GCE/bCNT-ssDNA.

The results presented here were obtained using three different dispersions and three electrodes in each case.

2.4.2. UV–Vis experiments

The intercalation of PMZ within dsDNA was evaluated by UV–Vis spectroscopy using a quartz cuvette of 0.1 cm optic way. To study the PMZ–dsDNA and PMZ–ssDNA interaction in solution, the desired amount of PMZ was added to a 100 ppm DNA solution prepared in aqueous 0.200 M acetate buffer solution pH 5.00 or in a mix of such buffer with a 50% v/v ethanol:water solution, and was allowed to interact for 5.0 min (in order to emulate the DPV interaction conditions). The spectra were recorded between 200 and 600 nm.

To study the interaction of PMZ with the dsDNA that supports the bCNTs, a previous step was required for immobilizing the dispersion. The cuvette was sonicated in a 7.0% w/v NaOH solution (prepared in a 10.0% v/v ethanol–water mixture), followed by the assembling of a 0.50 mg mL^{-1} quaternized chitosan [35] prepared in 0.050 M phosphate buffer solution pH 7.40 for 30 min. This highly positively charged polymer reverses the silicate negative charges generated on the cuvette, providing the anchor points for immobilizing the negatively charged bCNT-dsDNA dispersion. After careful rinsing of the quaternized chitosan immobilized cuvette, the bCNT-dsDNA dispersion was assembled for 60 min. The interaction with PMZ was performed for 5.0 min and after that, the cuvette was carefully rinsed with 0.200 M acetate buffer solution pH 5.00 to remove any weakly bound PMZ. UV–Vis spectra were taken after each step during the building of the supramolecular architecture. Further details about the UV–Vis experiments can be found in the Supplementary information.

2.4.3. Computational method

Molecular modeling is a powerful tool for analyzing the interactions in biomolecular systems. The treatment of complex molecular systems requires the use of molecular mechanics methods, which present a low computational demand and good accuracy. In these methods the description of the electronic structure of extended molecules is considered constant through the entire simulation. Therefore, it is impossible to describe the optical properties or charge transfer processes, among other features, and it is necessary to use quantum chemical methods.

The characterization of the intercalation of different molecules within DNA at atomistic level is a challenging task since it requires an accurate description of weak intermolecular interactions of DNA base pairs. In the last decades, Density Functional Theory (DFT) has been one of the most used tools to represent the ground state electronic structure of a wide variety of molecular systems due to the accuracy of DFT calculations that might be compared to *ab-initio* methods with lower computational cost. DFT has drawbacks in the proper description of London dispersion forces; however, this deficiency may be easily overcome by the introduction of an empirical corrective term (DFT-D).

To properly describe London dispersion forces and study the intercalation of PMZ into DNA oligomers, in this work we used an approach named Self-Consistent-Charges Density Functional Tight-Binding with empirical correction for dispersion energy (SCC-DFTB-D) [36]. The SCC-DFTB is based on the expansion of the Kohn–Sham energy functional up to second order with respect to a reference electron density for the neutral atoms [37]. This method may be considered as an intermediate step between a full *ab-initio* calculation, where exchange and correlation energy are accounted in a simpler semi-empirical method.

The DFTB+ code [38] was used to obtain the optimization of the geometries as well as the calculations of the Hamiltonian, overlap matrix and the initial single electron density matrix. For the calculations performed here, we have used the *mio-1-1* parameter set for elements H, O, N, C and S [37,39,40].

This method is extended to the time-dependent SCC-DFTB (TD-DFTB) [41–43] to obtain the excited state properties of the system by applying a perturbation in the shape of a Dirac delta pulse to the initial ground state density matrix previously obtained [37]. After the pulse application, the density matrix evolves in time and its evolution can be calculated by time integration of the Liouville–von Neumann equation of motion in the non-orthogonal basis, according to Eq. (3):

$$\frac{\partial \hat{\rho}}{\partial t} - \left[S^{-1}\hat{H}[\rho]\hat{\rho} - \hat{H}[\rho]\hat{\rho}S^{-1}\right] \tag{3}$$

where $\hat{\rho}$ is the single electron density matrix, S is the overlap matrix and $\hat{H}$ is the SCC-DFTB Hamiltonian. Within the linear response regime, when the applied electric field is small, the response is linear and the dipole moment is given by the Eq. (4):

$$\mu(t) - \int \alpha(t-\tau)E(\tau)d\tau \tag{4}$$

where $\alpha(t-\tau)$ is the polarizability along the axis over which the external field $E(\tau)$ is applied. The absorption spectrum is proportional to the imaginary part of the frequency dependent polarizability (Eq. (5)), obtained from the Fourier transform of the time-dependent dipole moment, after the deconvolution of the applied electric field.

$$\alpha(\omega) - \frac{\mu(\omega)}{E(\omega)}. \tag{5}$$

This method has been successfully used to calculate the optical properties of photosynthetic pigments [41,44] and organic molecules adsorbed onto TiO_2 nanoparticles [45]. In these previous reports we showed that TD-DFTB based spectra showed a remarkable agreement with the experiment, even better than the ones obtained by TD-DFT.

In the quantum dynamics simulation, we used a dsDNA octamer 5′-d[CCTCGTCC]-3′ as model dsDNA species. The intercalation site is located between the 4th and 5th base pair, that is, in a pyrimidine–purine base-pair step. Fig. S5 (in Supplementary information) shows the structure of the former octamer, both with and without the intercalation of PMZ.

3. Results and discussion

3.1. Electrochemical characterization of PMZ–DNA interaction

Fig. 1 shows the CV response of 1.0×10^{-4} M PMZ at different electrodes: GCE (a), GCE/bCNT (b), GCE/bCNT-dsDNA (c) and GCE/bCNT-ssDNA (d). At GCE there are two anodic peaks at 0.638 V and 0.810 V (vs. Ag/AgCl) associated with the irreversible cleavage of the lateral chain of PMZ and the formation of the phenothiazinium radical cation (Scheme 2). After reversing the scan at 0.900 V, two cathodic peaks, related to the reversible redox processes of the phenothiazinium radical cation, appear at 0.386 V and 0.038 V (vs. Ag/AgCl) [46]. It is important to mention that if the scan is reversed at 0.700 V, no changes were observed in these cathodic peaks, indicating that these processes depend on the PMZ oxidation product generated at 0.638 V (not shown).

At GCE/bCNT (b) there is a decrease in the overvoltage for the primary oxidation of PMZ compared to bare GCE ((0.58 ± 0.06) vs (0.638 ± 0.002) V (vs. Ag/AgCl) for GCE/bCNT and GCE, respectively) as well as a significant increase in the associated current density (4.1 times), clearly proving the catalytic activity of bCNTs. The linear relationship between the oxidation peak current of PMZ and the scan rate (between 0.010 and 0.400 V·s^{-1}) demonstrated an adsorptive behavior at GCE/bCNTs (not shown). Considering that PMZ is spontaneously

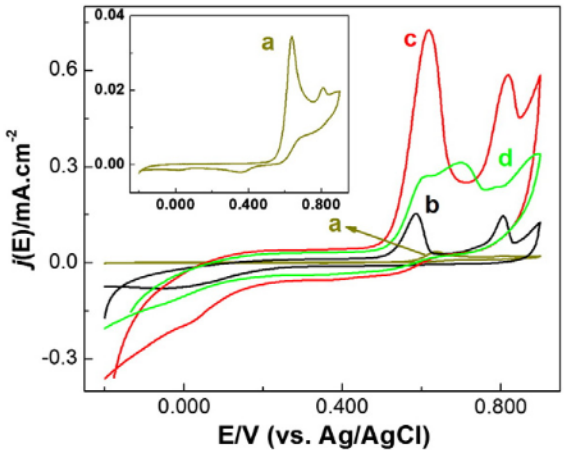

Fig. 1. CV responses over (a) GCE, (b) GCE/bCNT, (c) GCE/bCNT-dsDNA and (d) GCE/bCNT-ssDNA, obtained in a 1.0×10^{-4} M PMZ solution. Supporting electrolyte: 0.200 M acetate buffer solution pH 5.00. $\nu = 0.010\ V \cdot s^{-1}$.

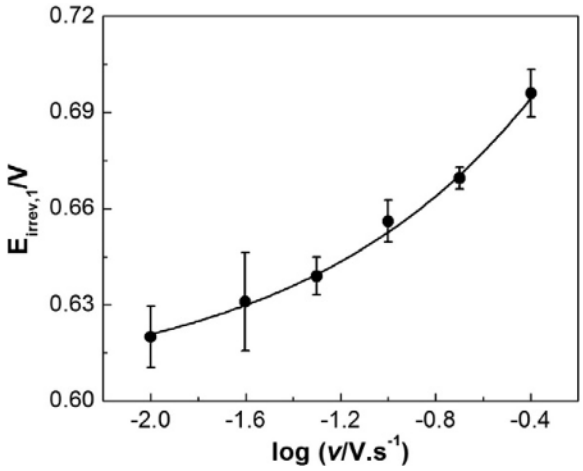

Fig. 2. Peak potential of the first oxidation process ($E_{irrev,1}$) as a function of the logarithm of the scan rate (ν) for the CV responses at GCE/bCNT-dsDNA obtained in a 1.0×10^{-4} M PMZ solution at various scan rates. The CVs are shown in Fig. S1, in the Supplementary information.

adsorbed at GCE/bCNT, the increase in the oxidation current at GCE/bCNT is not only due to the PMZ that diffuses from the bulk of the solution but also to the pre-accumulated one (additional results about the adsorption of PMZ at GCE/bCNT will be discussed below). The voltamperometric profile obtained at GCE/bCNT-dsDNA (c) shows an increment even more important in the oxidation current (19.7 and 4.9 times compared to GCE and GCE/bCNT, respectively), indicating that PMZ can be accumulated not only due to the adsorptive effect of bCNTs, but also to the preconcentration within the dsDNA that supports the bCNTs. To evaluate the influence of the double helix in the interaction with PMZ, we studied the voltamperometric behavior of PMZ at a GCE modified with bCNT dispersed in ssDNA (d). The j–E profile shows a broad peak that involves several anodic processes, with current densities higher than those obtained at GCE/bCNT but considerably smaller than the ones obtained at GCE/bCNT-dsDNA. These multiple electrochemical processes can be attributed to the reaction of phenothiazinium radical cation with the disordered ssDNA layer since it presents a high binding activity towards the unpaired nucleotides [26].

The effect of the scan rate on the PMZ oxidation-peak potential (E_p) was also evaluated at the different electrodes. At GCE/bCNT there is a linear relationship between $E_p/(V)$ (vs. Ag/AgCl) vs $\log \nu/(V \cdot s^{-1})$ indicating that the process correspond to the oxidation of an irreversibly adsorbed species (not shown). On the contrary, the plot of $E_p/(V)$ (vs. Ag/AgCl) vs $\log \nu/(V \cdot s^{-1})$ for GCE/bCNT-dsDNA suggests a typical behavior of a thin-film redox couple (Fig. 2) [47], indicating that PMZ strongly interacts with the dsDNA that supports the bCNT and presents an electrochemical behavior similar to the one of a redox compound confined in a finite length (diffusionless) [48,49]. This different behavior in the electrochemical behavior of PMZ at GCE/bCNT and GCE/bCNT-dsDNA clearly proves that the origin of such variation is due to the presence of dsDNA. In the case of GCE/bCNT-ssDNA, since the electrochemical response is the convolution of several oxidation processes, it was not possible to obtain the E_p values in a clear way.

In order to evaluate more clearly the interaction between PMZ and GCE/bCNT-dsDNA we performed DPV-adsorptive stripping experiments with medium exchange. Fig. 3 displays DPVs obtained in a 0.200 M acetate buffer solution pH 5.00 after 5.0 min interaction of 5.0×10^{-6} M PMZ at GCE/bCNT-dsDNA (A) and GCE/bCNT-ssDNA (B) and medium exchange previous rinsing with 0.200 M acetate buffer solution pH 5.00 (solid lines). The current density for the oxidation of PMZ at GCE/bCNT-dsDNA is considerably higher than the one obtained at GCE/bCNT-ssDNA ((1.76 ± 0.03) vs $(0.15 \pm 0.02)\ mA \cdot cm^{-2}$, respectively), in agreement with the CV results previously shown. Since DNA bears a negative charge density due to the presence of the phosphate backbone, an electrostatic attraction with PMZ (pKa = 9.1) is expected either with ss or dsDNA. However, in the case of the interaction between PMZ and the dsDNA that support the bCNTs there must be another contribution besides the electrostatic one, which is responsible for the important increase in the current density obtained at bCNT-dsDNA.

To demonstrate this behavior, the effect of the ionic strength on the interaction of PMZ was evaluated by performing DPV stripping experiments similar to those shown in Fig. 3 (solid line), but rinsing the electrode containing the accumulated PMZ with a 0.200 M NaCl solution (prepared in 0.200 M acetate buffer solution pH 5.00) instead of the acetate buffer alone. Under these conditions, at GCE/bCNT-dsDNA the

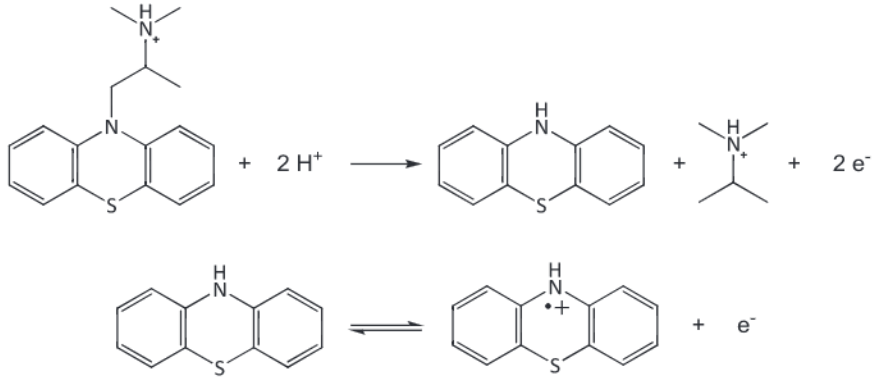

Scheme 2. Electrochemical reaction of PMZ.

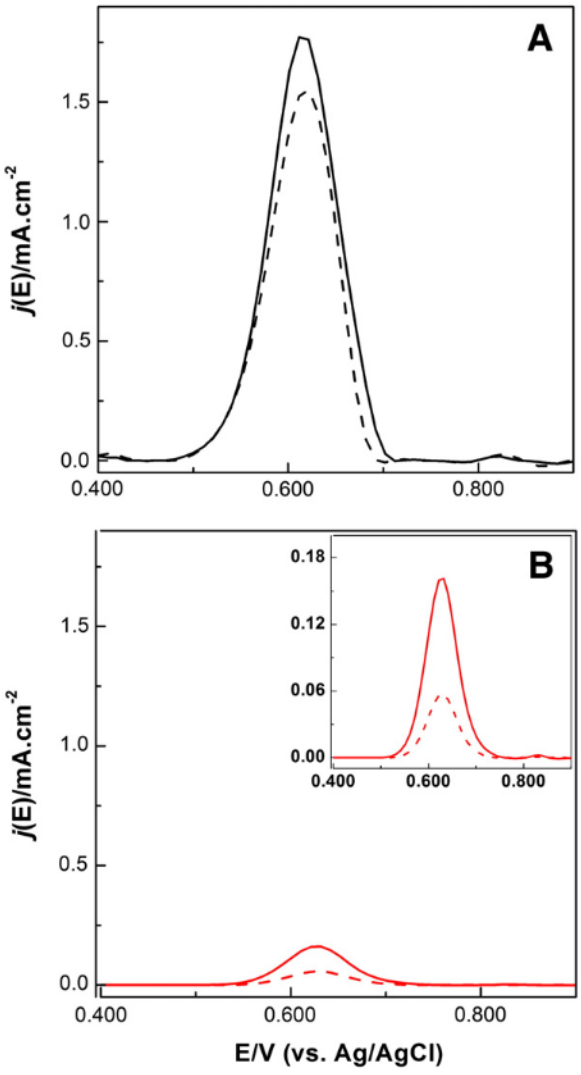

Fig. 3. Differential pulse voltamperometric responses (with their baselines subtracted) over (A) GCE/bCNT-dsDNA and (B) GCE/bCNT-ssDNA obtained after accumulation at open circuit potential in a 5.0×10^{-6} M PMZ solution for 5.0 min and rinsing in acetate buffer solution (full lines) or a 0.200 M NaCl solution (dashed lines). Supporting electrolyte: 0.200 M acetate buffer solution pH 5.00. The inset in panel B depicts a zoom.

oxidation current of PMZ decreases just 11% ((1.76 ± 0.03) versus (1.55 ± 0.05) mA·cm^{-2}) (Fig. 3A, dashed line), while in the case of GCE/bCNT-ssDNA containing PMZ, upon rinsing with the NaCl solution (Fig. 3B, dashed line), the oxidation current of PMZ decreases 60% ((0.15 ± 0.02) versus (0.063 ± 0.002) mA·cm^{-2}), evidencing that the main interaction mode between PMZ and the ssDNA that supports the bCNTs in GCE/bCNT-ssDNA is electrostatic. Analog DPV experiments performed at GCE/bCNT gave similar currents by washing the electrode containing PMZ either with acetate buffer or with the NaCl solution ((0.424 ± 0.009) versus (0.41 ± 0.01) mA·cm^{-2}, respectively), as expected for the hydrophobic interaction of PMZ with the CNTs walls (not shown). These results reinforce the conclusion that, although electrostatics plays some role in the interaction between PMZ and bCNT-dsDNA due to the presence of the phosphate groups, van der Waals interactions between the DNA bases and PMZ, which are independent on the salt concentration of the medium, are the main responsible for the PMZ oxidation current.

Since the bCNTs deposited at GCE form a porous film that allows the flux of electrolyte and solvent, it is possible to understand the nature of the interactions between PMZ and bCNTs and/or dsDNA by measuring the interfacial properties of the platforms. Therefore, the layer's specific capacitance can be used to characterize the accessible surface area in these porous materials. Table 1 shows the capacitances obtained in acetate buffer in the absence and in the presence of PMZ at GCE modified with bCNT, bCNT-ssDNA and bCNT-dsDNA. The capacitance obtained for GCE/bCNT in acetate buffer ((1.81 ± 0.02) mF·cm^{-2}) agrees with the values previously reported for other CNT-based electrodes [50]. When bCNTs are dispersed, either in ssDNA ((3.64 ± 0.02) mF·cm^{-2}) or in dsDNA ((4.23 ± 0.05) mF·cm^{-2}) the capacitances increase, confirming the formation of an even more porous deposit over the electrode due to a better exfoliation of the nanotubes. It is widely known that upon increasing the porosity of an electroactive substrate in contact with an electrolyte, the capacitance also increases. In the case of CNTs deposited at GCE, this increase is related to a better dispersion of them which leaves a major density of pores and/or to a reduction in the hydrophobicity of the surface because of the presence of the bio-polymer (DNA), which allows the flux of ions and water molecules [51].

The capacitance also gives information about the dielectric properties of the interface, since it can be defined, in the most simple model, like a parallel-plate capacitor of capacitance $C = \varepsilon_0\varepsilon_{dl}/\delta$ (where: ε_0 is the vacuum's permittivity; ε_{dl}, the dielectric constant of the interface and δ, the thickness of the double layer) [33]. The capacitances for GCE/bCNT and GCE/bCNT-ssDNA decrease 8.3% and 9.3%, respectively, after interaction with PMZ (Table 1). This decrease can be attributed to the adsorption of PMZ at the bCNTs and/or to the electrostatic interaction with the ssDNA forming a layer over the surface of the film. As PMZ is an organic insulator, it produces a decrease in the dielectric constant of the interface and the consequent reduction in the capacitance. Similar results can be found when modifying any conducting substrate with an organic insulating layer [52]. On the contrary, after the interaction of PMZ with dsDNA that supports the bCNTs at GCE/bCNT-dsDNA, the capacitance increases by 21.0%, clearly indicating a differential affinity between this platform and PMZ. In this sense, it is important to remark that, as we previously demonstrated [14], although the wrapping of DNA around the bCNTs occurs due to a partial denaturation, there are zones of the DNA that remain with the double helix structure exposed to the solution, leaving some regions of the bCNTs uncovered.

At this point it is clear that, in addition to the electrostatic one, there is another interaction (of hydrophobic nature) between PMZ and the dsDNA that support the bCNTs, which is responsible for the increased accumulation properties, the distinctive electrochemical behavior and the characteristic variation in the interfacial permittivity.

3.2. Spectroscopic study versus quantum dynamic calculations at DFTB level of PMZ–DNA interaction

UV–Vis spectroscopy studies and quantum dynamics calculations at DFTB level were performed to critically evaluate the intercalation of PMZ within dsDNA. Fig. 4 compares the experimental UV–Vis spectra for dsDNA (A) and PMZ (C) with those calculated using the TD-DFTB method previously described (B and D, for dsDNA and PMZ, respectively). The experimental spectrum of dsDNA (Fig. 4A) shows a broad peak at 260 nm, which corresponds to the π–π* electronic transitions of the 4 bases. The calculated spectrum presents a red-shift of approximately 7 nm in the maximum absorption wavelength (Fig. 4B), attributed to

Table 1
Double layer specific capacitances (C) obtained by performing CV experiments at various scanning rates (ν) and plotting the non-faradaic current density ($j_{n\text{-}f}$/mA·cm^{-2}) (at E = 0.360 V) vs. (ν/V·s^{-1}), according to $C = (\partial j_{n\text{-}f}/\partial\nu)$. The plots are shown in Fig. S2, in the Supplementary information.

Electrode	C/mF·cm^{-2}	
	In 0.200 M acetate buffer pH 5.00	In 1.0×10^{-4} M PMZ
GCE/bCNT	1.81 ± 0.02	1.66 ± 0.04
GCE/bCNT-dsDNA	4.23 ± 0.05	5.12 ± 0.03
GCE/bCNT-ssDNA	3.64 ± 0.02	3.3 ± 0.1

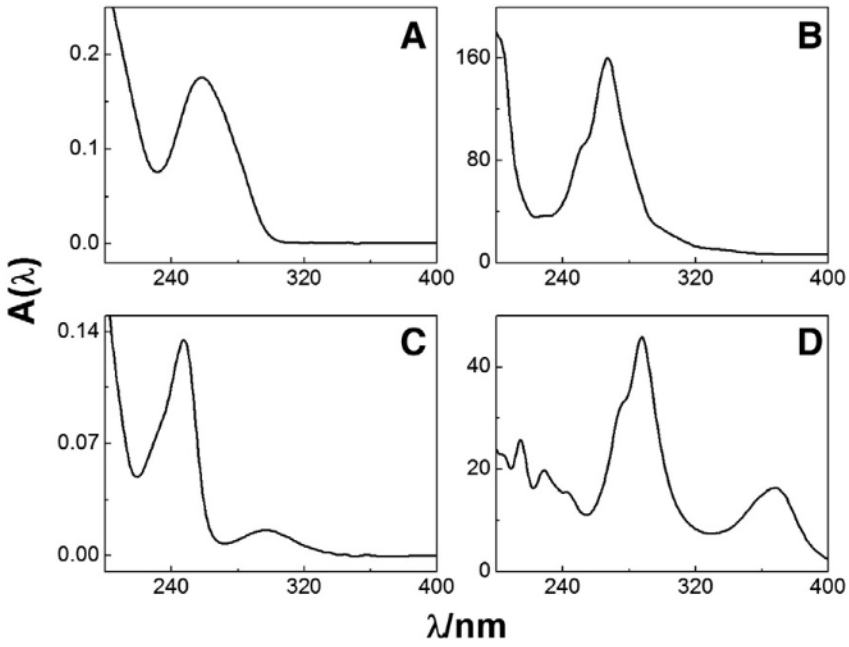

Fig. 4. Absorption spectra for (A) 100 ppm dsDNA solution and (B) the calculated one; (C) 5.0×10^{-5} M PMZ solution and (D) the calculated one.

the size differences between the DNA used for the calculation and calf-thymus dsDNA (c.a. 50 kbp), since a large amount of base pairs produce many π–stacking interactions that stabilize the ground state and increase the electronic excitation energy. The experimental spectrum of PMZ (Fig. 4C) shows two absorption bands, at 249.8 nm and 298.5 nm. The last one, due to π–π* electronic transition of the conjugated aromatic ring, was used to evaluate the interaction with dsDNA.

When comparing the calculated and the experimental spectra for PMZ, the maximum absorption wavelength is red-shifted by approximately 60 nm (Fig. 4D). Such discrepancy can be attributed to two different factors: i) The fact that the theoretical absorption spectrum of PMZ was calculated in the vacuum while the experimental absorption spectrum was obtained in acetate buffer solution, where the solvent might have some stabilization effect on the ground state of the molecule; ii) The underestimation of the excitation energy by TD-DFTB. To make sure that this underestimation is not related to the parametrization of our method, we compared our result with that obtained by standard TD-DFT at B3PW91/6-31 + G(d) level implemented in the Gaussian 09 program package [53]. The second band was obtained at 397.3 nm, this energy value being 99 nm larger than the experimental one, indicating that TD-DFT exhibits less accuracy than our methodology.

It is important to remark that we are interested in the qualitative aspects of the optical spectra, since the aim of the computational method is to complement the experimental results in order to determine whether the molecule is intercalated or not in the dsDNA. Considering that the intercalation involves π–stacking between the base pairs and the ligand, the main variation in the absorption spectrum of the dsDNA + PMZ that we would expect is in the π–π* electronic transition of the ligand (the calculated π and π* molecular orbitals are shown in Fig. S3).

In order to evaluate the intercalation of PMZ within the dsDNA, the UV–Vis spectrum for a 5.0×10^{-4} M PMZ was obtained in the presence of dsDNA (in solution). Due to the overlapping of PMZ and dsDNA absorption bands, the dsDNA spectrum was subtracted from that of PMZ + dsDNA mix (additional details regarding the subtraction procedure can be found in the Supplementary information, Section 3.2). Fig. 5A displays the region of the PMZ spectrum around 300 nm (a) and the subtracted signals due to PMZ in the presence of dsDNA (b) and ssDNA (c). Upon interacting with dsDNA, the PMZ maximum absorption wavelength is shifted from 298.5 to 302.0 nm and the absorbance slightly decreases. This displacement can be attributed to the change in the effective dielectric constant of the surroundings of the

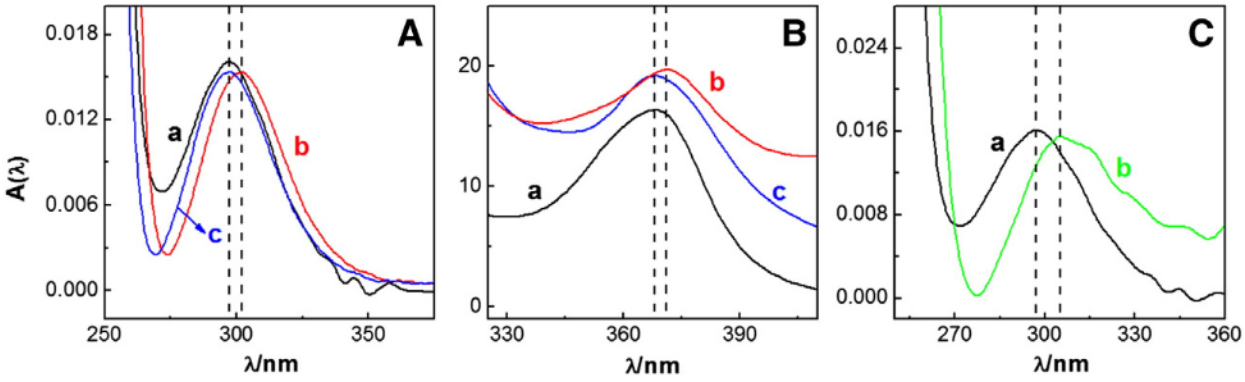

Fig. 5. Panel A corresponds to the absorption spectra for (a) a 5.0×10^{-5} M PMZ solution and the subtracted UV–Vis spectra a 5.0×10^{-5} M PMZ solution after 5 min of interaction with (b) 100 ppm dsDNA solution and (c) 100 ppm ssDNA solution. Panel B corresponds to the calculated spectra of PMZ under the same conditions as in A. Panel C shows the experimental absorption spectra for (a) a 5.0×10^{-5} M PMZ solution and (b) the subtracted UV–Vis spectra a 5.0×10^{-5} M PMZ solution after 5 min of interaction with bCNT/dsDNA supported over the quartz cuvette. The dashed vertical lines represent the position of the different absorption maxima.

molecule (when comparing to the free PMZ in solution), which produces a decrease in the energy of the π electrons and the consequent bathochromic shifting in the PMZ spectrum. As it is shown in Fig. 5A (c), practically no changes are observed in the presence of ssDNA.

Fig. 5B depicts the theoretical spectra of free (a) and intercalated (b) PMZ. There is a shifting from 367.6 to 370.4 nm, in agreement with the experimental results. No shifting was observed in the band at 367.6 nm when comparing the theoretical spectrum of free PMZ (a) and the one obtained for the interaction of PMZ with ssDNA (c) (see Fig. S6 in the Supplementary information for the minimized structure of ssDNA + PMZ). This behavior is similar to the one observed with other intercalators [54–56] and clearly shows that PMZ can be intercalated within the dsDNA.

To demonstrate the intercalation of PMZ within the dsDNA that supports the bCNTs, we immobilized the bCNT-dsDNA dispersion on the quartz cuvette and then it was left to interact with PMZ. The spectrum obtained in 0.200 M acetate buffer solution pH 5.00 shows a red-shift of the maximum absorption wavelength from 298.5 nm to 305.2 nm upon the interaction with PMZ (Fig. 5C (a) vs 5C (b)). This bathochromic displacement of 6.7 nm is attributed to the intercalation of PMZ. Compared to the spectra obtained after the interaction of PMZ with native dsDNA, there is an additional shifting which can be attributed to the different environments where PMZ is located, which would produce additional changes in the molecule's surroundings effective dielectric constant.

The intercalation of PMZ within the dsDNA that supports bCNTs demonstrated above allows us to explain the unusual increase in the capacitance of GCE/bCNT-dsDNA (21.0%) upon interacting with PMZ, shown in Section 3.1. As a consequence of the intercalation, the double helix of DNA undergoes elongation to reduce the tension, and the hydrodynamic properties and the viscosity of the DNA strand change [57]. Therefore, some distortion could occur in the double stranded portion that supports the bCNTs making the polymer film more permeable to the flux of water and supporting electrolyte ions. These physical changes and the consequent increment in the permeation of the polymer suggest an increase in the ε_{dl} and could explain the growth in the capacitance when PMZ is present at the GCE/bCNT-dsDNA.

3.3. Analytical performance of GCE/bCNT-dsDNA for the quantification of PMZ

Owing to the facile collection of PMZ by the surface-confined bCNT-dsDNA layer, the effective preconcentration step prior to the electrochemical measurement was used for the analytical determination of PMZ.

In order to select the interaction time of PMZ with bCNT-dsDNA, we studied the influence of the accumulation time upon the DPV response. The PMZ oxidation current increased rapidly with the preconcentration time at first (up to 3.0 min) and then it leveled off (not shown). The selected time was 5.0 min.

Fig. 6 displays the calibration plots for PMZ obtained in a 0.200 M acetate buffer solution pH 5.00 after 5.0 min interaction of GCE/bCNT-dsDNA (empty circles) and GCE/bCNT-ssDNA (full circles) with increasing concentration of PMZ. Table 2 shows the analytical parameters of the calibration plots for both bioelectrodes. The increase of the sensitivity for GCE/bCNT-dsDNA in one order of magnitude when compared to GCE/bCNT-ssDNA confirms once more that the specific interaction between PMZ and the dsDNA that supports the bCNTs gives special accumulation properties and better analytical performance to the modified GCE/bCNT-dsDNA, allowing the nanomolar detection of PMZ.

Table 3 compares the analytical performance of this biosensor with those obtained for other PMZ electrochemical sensors using CNTs and/or dsDNA. The results demonstrate that our (bio)sensor is highly competitive in terms of linear range and detection limit, making possible the sensitive quantification of PMZ, with detection limits comparable to or even better than those obtained with the other strategies,

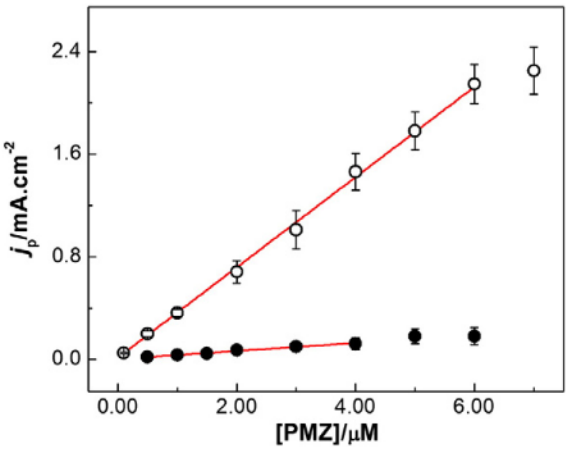

Fig. 6. Calibration plots obtained over (●) GCE/bCNT-ssDNA and (○) GCE/bCNT-dsDNA by the peak current density (j_p) of DPV recordings' previous accumulation in the corresponding PMZ solution and rinsing the electrode with acetate buffer solution. Supporting electrolyte: 0.200 M acetate buffer solution pH 5.00. The analytical parameters from the lineal fittings (shown in red lines) are presented in Table 2. GCE/bCNT-ssDNA: $j_p([PMZ]) = (0.031 \pm 0.002)$ [PMZ]. GCE/bCNT-dsDNA: $j_p([PMZ]) = (0.350 \pm 0.005)$ [PMZ] + (0.014 ± 0.006).

with exception of [58]. In the latter case, the authors used the preconcentration properties of the dsDNA adsorbed at graphite paste electrode as sensing layer, although the transduction was performed with constant current potentiometric stripping analysis, an extremely sensitive technique that presents an excellent system of filters and base line correction.

The GCE/bCNT-dsDNA was challenged with a pharmaceutical product containing PMZ as active component (*Prometazina Cevallos*). The calculated value was (51.30 ± 0.05) mg in 2 mL, while the reported one is 50 mg of PMZ in 2 mL. Therefore, the methodology proposed here is useful to detect PMZ in a real sample with excellent agreement (2.6%).

4. Conclusions

The presence of bCNTs-dsDNA at the surface of GCE improves the charge transfer of PMZ due to the catalytic effect of CNTs and the favorable interaction of PMZ with dsDNA. DPV adsorptive stripping with medium exchange experiments showed that promethazine interacts with the dsDNA layer that supports the bCNTs mainly by intercalation within the double helix, demonstrating that, even after the drastic conditions for preparing the dispersion of bCNT in dsDNA, this biomolecule keeps the bioaffinity properties. Spectroscopic measurements and quantum dynamics calculations at DFTB level confirmed that PMZ intercalates within the dsDNA that supports bCNT. The strong interaction of PMZ at GCE/bCNT-dsDNA makes possible an efficient preconcentration at the electrode surface that largely improves the sensitivity and detection limits down to nanomolar levels.

It is important to remark that the resulting GCE/bCNT-dsDNA represents a new alternative to build supramolecular architectures for

Table 2
Analytical parameters obtained from the calibration plots shown in Fig. 6 for the determination of PMZ.

Analytical parameter	GCE/bCNT-ssDNA	GCE/bCNT-dsDNA
Sensitivity/μA·cm^{-2}·M^{-1}	$(3.1 \pm 0.2) \times 10^7$	$(3.50 \pm 0.05) \times 10^8$
R[2a]	0.95	0.998
Linear range/μM	0.50–4.0	0.10–6.0
LOD/μM[b]	0.34	0.023

[a] Correlation coefficient.
[b] LOD (detection limit) was calculated as 3σ/s, where σ is the standard deviation of the blank signal and s is the sensitivity.

Table 3
Comparative data of different electrochemical interfaces for the quantification of PMZ.

Platform and conditions	Technique	Linear range/M	LOD/M	Samples	Ref.
CPE/dsDNA (3 min accumulation at controlled potential)	PSA	$0.20–1.40 \times 10^{-7}$	5×10^{-9}	–	[58]
AuE/cysteamine/glutaraldehyde/cysteamine/AuNps/dsDNA (3 min accumulation at controlled potential)	DPV	$2–16 \times 10^{-5}$	1×10^{-5}	–	[30]
CPE/CNT-ethylendiamine/dsDNA (3 min accumulation at open circuit potential)	SWV	$2.5 \times 10^{-8}–2.1 \times 10^{-6}$	–	–	[31]
AuE/MWCNTs (2 min accumulation at controlled potential)	CV	$5.0 \times 10^{-8}–1.0 \times 10^{-5}$	1.0×10^{-8}	Pharmaceutical sample	[59]
Boron-doped diamond electrode (30 s accumulation at controlled potential)	SWV	$5.96 \times 10^{-7}–4.76 \times 10^{-6}$	2.66×10^{-8}	Pharmaceutical sample	[60]
Composite electrode made of MWCNT, SiO_2, Nb_2O_5 and dsDNA	SWV	$20–100 \times 10^{-6}$	5.9×10^{-6}	Pharmaceutical sample	[29]
GCE/bCNT-dsDNA (5 min accumulation at open circuit potential)	DPV	$0.1–6.0 \times 10^{-6}$	2.3×10^{-8}	Pharmaceutical sample	This work

Symbols: PSA, potentiometric stripping analysis; SWV, square wave voltammetry; CPE, carbon paste electrode; AuE, gold electrode; Nps, nanoparticles.

biosensing, opening the doors to new and exciting possibilities for the development of biosensors based on nanomaterials using different biorecognition molecules.

Acknowledgments

The authors thank CONICET, MINCyT-Córdoba, SECyT-UNC and ANPCyT for the financial support. CCAD-UNC and GPGPU Computing Group-FaMAF-UNC are acknowledged for providing the computational resources. E. N. P. and M. B. O. thank CONICET for their fellowships.

Appendix A. Supplementary data

Supplementary data to this article can be found online at http://dx.doi.org/10.1016/j.bioelechem.2014.05.002.

References

[1] J.K. Wassei, R.B. Kanner, Oh, the places you'll go with graphene, Acc. Chem. Res. 46 (2013) 2244–2253.
[2] X.-Q. Zhang, X. Xu, N. Bertrand, E. Pridgen, A. Swami, O.C. Farokhzad, Interactions of nanomaterials and biological systems: implications to personalized nanomedicine, Adv. Drug Deliv. Rev. 64 (2012) 1363–1384.
[3] R.C. McIntyre, Common nano-materials and their use in real world applications, Sci. Prog. 95 (2012) 1–22.
[4] E. Heister, E.W. Brunner, G.R. Dieckmann, I. Jurewicz, A.B. Dalton, Are carbon nanotubes a natural solution? Applications in biology and medicine, ACS Appl. Mater. Interfaces 5 (2013) 1870–1891.
[5] C.I.L. Justino, T.A.P. Rocha-Santos, A.C. Duarte, Advances in point-of-care technologies with biosensors based on carbon nanotubes, Trends Anal. Chem. 45 (2013) 24–36.
[6] Q. Zang, J.-Q. Huang, W.-Z. Qian, Y.-Y. Zhang, F. Wei, The road for nanomaterials industry: a review of carbon nanotube production, post-treatment, and bulk applications for composites and energy storage, Small 9 (2013) 1237–1265.
[7] L.Y. Heng, A. Chou, J. Yu, Y. Chen, J.J. Gooding, Demonstration of the advantages of using bamboo-like nanotubes for electrochemical biosensor applications compared with single walled carbon nanotubes, Electrochem. Commun. 7 (2005) 1457–1462.
[8] M. Lin, J.P.Y. Tan, C. Boothroyd, K.P. Loh, E.S. Tok, Y.-L. Foo, Dynamical observation of bamboo-like carbon nanotube growth, Nano Lett. 7 (2007) 2234–2238.
[9] G.A. Rivas, M.D. Rubianes, M.C. Rodriguez, N.F. Ferreyra, G.L. Luque, M.L. Pedano, S.A. Miscoria, C. Parrado, Carbon nanotubes for electrochemical biosensing, Talanta 74 (2007) 291–307.
[10] P. Yáñez-Sedeño, J. Riu, J.M. Pingarrón, F.X. Rius, Electrochemical sensing based on carbon nanotubes, Trends Anal. Chem. 29 (2010) 939–953.
[11] C. Gao, Z. Guo, J.-H. Liu, X.-J. Huang, The new age of carbon nanotubes: an updated review of functionalized carbon nanotubes in electrochemical sensors, Nanoscale 4 (2012) 1948–1963.
[12] T. Premkumar, R. Mazzenga, K.E. Geckeler, Carbon nanotubes in the liquid phase: addressing the issue of dispersion, Small 8 (2012) 1299–1313.
[13] C.I.L. Justino, T.A.P. Rocha-Santos, S. Cardoso, A.C. Duarte, Strategies for enhancing the analytical performance of nanomaterial-based sensors, Trends Anal. Chem. 47 (2013) 27–36.
[14] E.N. Primo, P. Cañete-Rosales, S. Bollo, M.D. Rubianes, G.A. Rivas, Dispersion of bamboo type multi-wall carbon nanotubes in double stranded calf- thymus DNA, Colloids Surf. B 108 (2013) 329–336.
[15] G.A. Rivas, M.L. Pedano, N.F. Ferreyra, Electrochemical biosensors for sequence-specific DNA detection, Anal. Lett. 38 (2005) 2653–2703.
[16] E. Palecek, M. Bartosik, Electrochemistry of nucleic acids, Chem. Rev. 112 (2012) 3427–3481.
[17] M. Fojta, Electrochemical sensors for DNA interactions and damage, Electroanalysis 14 (2002) 1449–1463.
[18] D. Kato, O. Niwa, Carbon-based electrode materials for DNA electroanalysis, Anal. Sci. 29 (2013) 385–392.
[19] M.-Y. Wei, L.-H. Guo, P. Famouri, DNA biosensors based on metallo-intercalator probes and electrocatalytic amplification, Microchim. Acta 172 (2011) 247–260.
[20] M. Lazerges, F. Bedioui, Analysis of the evolution of the detection limits of electrochemical DNA biosensors, Anal. Bioanal. Chem. 405 (2013) 3705–3714.
[21] A. Erdem, M. Ozsoz, Electrochemical DNA biosensors based on DNA–drug interactions, Electroanalysis 14 (2002) 965–974.
[22] C.V. Uliana, G.S. Garbellini, H. Yamanaka, Evaluation of the interactions of DNA with the textile dyes Disperse Orange 1 and Disperse Red 1 and their electrolysis products using an electrochemical biosensor, Sensors Actuators B Chem. 178 (2013) 627–635.
[23] P. Arias, N.F. Ferreyra, G.A. Rivas, S. Bollo, Glassy carbon electrodes modifies with CNT dispersed in chitosan: analytical applications for sensing DNA–methylene blue interaction, J. Electroanal. Chem. 634 (2009) 123–126.
[24] J. Wang, M. Chicharro, G. Rivas, X. Cai, N. Dontha, P.A.M. Farias, H. Shiraishi, DNA biosensor for the detection of hydrazines, Anal. Chem. 68 (1996) 2251–2254.
[25] K. Yang, C.-Y. Zhang, Simple detection of nucleic acids with a single-walled carbon-nanotube-based electrochemical biosensor, Biosens. Bioelectron. 28 (2011) 257–262.
[26] N.J. De Mol, A.B.C. Becht, J. Koenen, G. Lodder, Irreversible binding with biological macromolecules and effects in bacterial mutagenicity tests of the radical cation of promethazine and photoactivated promethazine. Comparison with chlorpromazine, Chem. Biol. Interact. 57 (1986) 73–83.
[27] K. Stolze, R.P. Mason, ESR spectroscopy of flow-oriented cation radicals of phenothiazine derivatives and phenoxathiin intercalated in DNA, Chem. Biol. Interact. 77 (1991) 283–289.
[28] J.P. Marco, K.B. Borges, C.R. Teixeira Tarley, E.S. Ribeiro, A.C. Pereira, Development of a simple, rapid and validated square wave voltametric method for determination of promethazine in raw material and pharmaceutical formulation using DNA modified multiwall carbon nanotube paste electrode, Sensors Actuators B Chem. 177 (2013) 251–259.
[29] J. Zhong, Z. Qi, H. Dai, C. Fan, G. Li, N. Matsuda, Sensing phenothiazine drugs at a gold electrode co-modified with DNA and gold nanoparticles, Anal. Sci. 19 (2003) 653–657.
[30] H. Tang, J. Chen, K. Cui, L. Nie, Y. Kuang, S. Yao, Immobilization and electro-oxidation of calf thymus deoxyribonucleic acid at alkylamine modified carbon nanotube electrode and its interaction with promethazine hydrochloride, J. Electroanal. Chem. 587 (2006) 269–275.
[31] R.Y. Hwang, G.-R. Xu, J. Han, J.Y. Lee, H.N. Choi, W.-Y. Lee, Determination of phenothiazine drugs using tris(2,2′-bipyridyl)ruthenium(II) electrogenerated chemiluminescence at DNA-modified electrode, J. Electroanal. Chem. 656 (2011) 258–263.
[32] L. Shapou, H. Xiaoli, L. Zhongfang, L. Ming, W. Fen, Study on the interactions of chlorpromazine hydrochloride and promethazine hydrochloride with nucleic acids by resonance Rayleigh scattering spectrum, Sci. China B 48 (2005) 591–599.
[33] A.J. Bard, L.R. Faulkner, Electrochemical Methods: Fundamentals and Applications, Wiley, New York, 2001.
[34] R.L. McCreery, Advanced carbon electrode materials for molecular electrochemistry, Chem. Rev. 108 (2008) 2646–2687.
[35] J. Desbrières, C. Martinez, M. Rinaudo, Hydrophobic derivatives of chitosan: characterization and rheological behaviour, Int. J. Biol. Macromol. 19 (1996) 21–28.
[36] M. Elstner, P. Hobza, T. Frauenheim, S. Suhai, E. Kaxiras, Hydrogen bonding and stacking interactions of nucleic acid base pairs: a density-functional-theory based treatment, J. Chem. Phys. 114 (2001) 5149–5155.
[37] M. Elstner, D. Porezag, G. Jungnickel, J. Elsner, M. Haugk, S. Suhai, G. Seifert, Self-consistent-charge density-functional tight-binding method for simulations of complex materials properties, Phys. Rev. B 58 (1998) 7260–7268.
[38] B. Aradi, B. Hourahine, T. Frauenheim, Initial steps towards automating the fitting of DFTB $E_{rep}(r)$, J. Phys. Chem. A 111 (2007) 5678–5684.
[39] T.A. Niehaus, M. Elstner, T. Frauenheim, S. Suhai, Application of an approximate density-functional method to sulfur containing compounds, J. Mol. Struct. THEOCHEM 541 (2001) 185–194.
[40] M. Gaus, Q. Cui, M. Elstner, DFTB3: extension of the self-consistent-charge density-functional tight-binding method (SCC-DFTB), J. Chem. Theory Comput. 7 (2012) 931–948.
[41] M.B. Oviedo, C.F.A. Negre, C.G. Sánchez, Dynamical simulation of the optical response of photosynthetic pigments, Phys. Chem. Chem. Phys. 12 (2010) 6706–6711.
[42] V.C. Fuertes, C.F.A. Negre, M.B. Oviedo, F.P. Bonafé, F.Y. Oliva, C.G. Sánchez, A theoretical study of the optical properties of nanostructured TiO_2, J. Phys. Condens. Matter 25 (2013) 115304.

[43] C.F.A. Negre, V.C. Fuertes, M.B. Oviedo, F.Y. Oliva, C.A.G. Sánchez, Quantum dynamics of light-induced charge injection in a model dye–nanoparticle complex, J. Phys. Chem. C 116 (2012) 14748–14753.
[44] M.B. Oviedo, C.G. Sánchez, Transition dipole moments of the Q_y band in photosynthetic pigments, J. Phys. Chem. A 115 (2011) 12280–12285.
[45] M.B. Oviedo, X. Zarate, C.F.A. Negre, E. Schott, R. Arratia-Pérez, C.G. Sánchez, Quantum dynamical simulations as a tool for predicting photoinjection mechanisms in dye-sensitized TiO_2 solar cells, J. Phys. Chem. Lett. 3 (2012) 2548–2555.
[46] B. Blankert, H. Hayen, S.M. van Leeuwen, U. Karst, E. Bodoki, S. Lotrean, R. Sandulescu, N. Mora Diez, O. Dominguez, J. Arcos, J.-M. Kauffmann, Electrochemical, chemical and enzymatic oxidations of phenothiazines, Electroanalysis 17 (2005) 1501–1510.
[47] E. Laviron, General expression of the linear potential sweep voltammogram in the case of difutionless electrochemical systems, J. Electroanal. Chem. 101 (1979) 19–28.
[48] S. Khezrian, A. Salimi, H. Teymourian, R. Hallaj, Label-free electrochemical IgE aptasensor based on covalent attachment of aptamer onto multiwalled carbon nanotubes/ionic liquid/chitosan nanocomposite modified electrode, Biosens. Bioelectron. 43 (2013) 218–225.
[49] Y. Dai, B. Chakraborty, B. Ge, H.Z. Yu, Adenosine-triggered elimination of methylene blue noncovalently bound to immobilized functional dsDNA-aptamer constructs, J. Phys. Chem. B 116 (2012) 6361–6368.
[50] J. Li, A. Cassell, L. Delzeit, j. Han, M. Meyyappan, Novel three-dimensional electrodes: electrochemical properties of carbon nanotubes ensembles, J. Phys. Chem. B 106 (2002) 9299–9305.
[51] P. Simon, A. Burke, Nanostructured carbons: double-layer capacitance and more, Interface 17 (2008) 38–43.
[52] A.L. Eckermann, D.J. Feld, J.A. Shaw, T.J. Meade, Electrochemistry of redox-active self-assembled monolayers, Coord. Chem. Rev. 254 (2010) 1769–1802.
[53] Gaussian 09, Revision A.01, M.J. Frisch, G.W. Trucks, H.B. Schlegel, G.E. Scuseria, M.A. Robb, J.R. Cheeseman, G. Scalmani, V. Barone, et al., Gaussian, Inc., Wallingford, 2009.
[54] M. Aslanoglu, G. Ayne, Voltammetric studies of the interaction of quinacrine with DNA, Anal. Bioanal. Chem. 380 (2004) 658–663.
[55] J. Lang, M. Liu, Layer-by-layer assembly of DNA films and their interactions with dyes, J. Phys. Chem. B 103 (1999) 11393–11397.
[56] L. Pérez-Flores, A.J. Ruiz-Chica, J.G. Delcros, F. Sánchez-Giménez, F.J. Ramírez, Intercalation and groove binding of an acridine-spermine conjugate on DNA sequences: an FT-Raman and UV–visible absorption study, J. Mol. Struct. 744–747 (2005) 699–704.
[57] D. Suh, J.B. Chaires, Criteria for the mode of binding of DNA binding agents, Bioorg. Med. Chem. 3 (1995) 723–728.
[58] J. Wang, G. Rivas, X. Cai, H. Shiraishi, P.A.M. Farias, N. Dontha, D. Luo, Accumulation and trace measurements of phenothiazine drugs at DNA-modified electrodes, Anal. Chim. Acta. 332 (1996) 139–144.
[59] P. Xiao, W. Wu, J. Yu, F. Zhao, Voltammetric sensing of promethazine on a multi-walled carbon nanotubes coated gold electrode, Int. J. Electrochem. Sci. 2 (2007) 149–157.
[60] F.W.P. Ribeiro, A.S. Cardoso, R.R. Portela, J.E.S. Lima, S.A.S. Machado, P. de Lima-Neto, D. de Souza, A.N. Correia, Electroanalytical determination of promethazine hydrochloride in pharmaceutical formulations on highly boron-doped diamond electrodes using square-wave adsorptive voltammetry, Electroanalysis 20 (2008) 2031–2039.